NDT&E International 43 (2010) 106–115

Contents lists available at ScienceDirect

NDT&E International

journal homepage: www.elsevier.com/locate/ndteint

Nondestructive evaluation of aircraft composites using reflective terahertz time domain spectroscopy

Christopher Stoik [a,*], Matthew Bohn [b,1], James Blackshire [c]

[a] Air Force Research Laboratory, Space Vehicles Directorate, 3550 Aberdeen Ave. SE, Kirtland AFB, NM 87117, USA
[b] Air Force Institute of Technology, Wright Patterson AFB, OH 45433, USA
[c] Air Force Research Laboratory, Materials and Manufacturing Directorate, Wright Patterson AFB, OH 45433, USA

ARTICLE INFO

Article history:
Received 27 April 2009
Received in revised form
24 September 2009
Accepted 24 September 2009
Available online 30 September 2009

Keywords:
Terahertz
Composites
Time domain spectroscopy
Dielectric properties
Terahertz imagery

ABSTRACT

Terahertz time domain spectroscopy in reflection configuration was assessed as a nondestructive evaluation technique for aircraft glass fiber composites. A technique for measuring the material properties of glass fiber composites using reflection geometry was demonstrated in addition to imaging of damaged glass fiber composites. Surface defects such as localized burn damage, puncture holes, and paint/composite removal were detected using amplitude and phase imaging methods. Hidden voids were also detected using the relative amplitude of the first Fabry–Perot reflection. The depths of discontinuities were then measured using a Fourier technique and then subtracting the incident pulse from the reflected pulse. Finally, nondestructive evaluation techniques for transmission and reflection configurations were compared.

Published by Elsevier Ltd.

1. Introduction

Glass fiber composites made from bundles of glass fiber imbedded in a polyimide resin are more frequently being used as structural components in high performance aircraft because of their high strength to weight ratios, improved aerodynamic performance, increased safety, and reduced corrosion compared with other structural materials. During the lifecycle of an aircraft, glass fiber composites can be weakened by various types of defects and stress, requiring complex maintenance techniques to repair them. Terahertz (THz) radiation has the unique ability to penetrate composites and identify defects such as voids, delaminations, punctures, mechanical damage, or heat damage [1–12]. THz offers a noninvasive, noncontact, nonionizing method of assessing composite part condition and could overcome some of the short-comings of microwaves, infrared, X-rays, and other nondestructive evaluation techniques.

THz Time Domain Spectroscopy (TDS) has been investigated as a possible method of the quality control and nondestructive evaluation of polymeric compounds and composites [6–11]. We examined aircraft glass fiber composites with various forms of damage with our THz TDS reflective configuration [12–14]. The first series of samples represent the outer shell of the panel of an aircraft, consisting mostly of the glass fiber composite with a thin outer coating. Refractive indices and absorption coefficients in the terahertz frequency range were measured using THz TDS in reflection configuration. Hidden voids and burn blisters could be located by TDS imaging using amplitude and phase analysis techniques. The depth of the delaminations could be measured via the timing of Fabry–Perot reflections after the main pulse. There was little evidence that areas of damage from bending stress and simulated hidden cracks (linear slit voids) could be detected with THz TDS reflective imaging. Finally, an entire glass fiber composite panel, consisting of a 2.5 cm honeycomb area sandwiched between two of the thin glass fiber composites tested earlier, was imaged. Surface damage such as punctures, paint removal, and burn areas were detected.

2. Theory and experiment

The THz TDS reflective setup used to collect the material parameter data and perform the imaging is shown in Fig. 1. A mode-locked, 100 fs, Ti:Sapphire laser drove a photoconductive switch biased with 48 V modulated at 50 kHz for detection using a lock-in amplifier. The THz pulse was reflected at 20° from the sample and was detected using an electro-optic technique (ZnTe

* Corresponding author.
E-mail addresses: christopher.stoik@kirtland.af.mil, afrl.rvse@kirtland.af.mil (C. Stoik).
[1] Currently at Directed Energy Solutions, Colorado Springs, CO 80907, USA.

0963-8695/$ - see front matter Published by Elsevier Ltd.
doi:10.1016/j.ndteint.2009.09.005

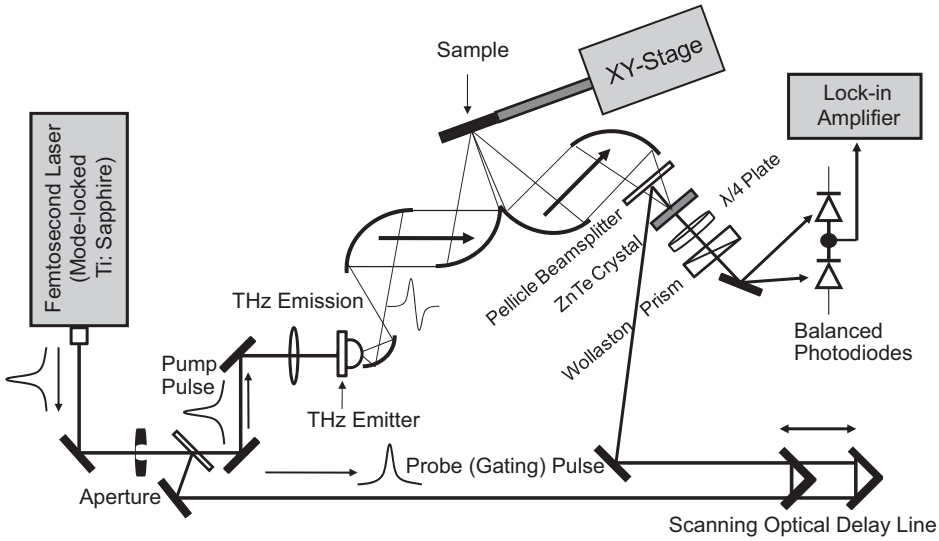

Fig. 1. THz TDS system used in reflection configuration for imaging and material parameter measurements.

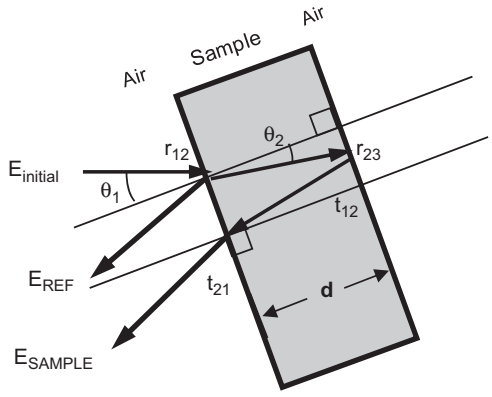

Fig. 2. Diagram showing the geometry of the surface reflection and the first Fabry–Perot reflection in THz TDS reflection configuration.

crystal). A Fourier transform could then be taken of the pulse to determine the amplitude spectrum of the THz pulse.

In reflection configuration, the index of refraction $n(\omega)$ could be calculated using the following equation:

$$n(\omega) = \frac{1 - |r(\omega)|^2}{1 + |r(\omega)|^2 - 2|r(\omega)|\cos\phi(\omega)} \tag{1}$$

where $|r(\omega)|$ is the ratio of the sample to the reference pulse and $\phi(\omega)$ the phase difference between the sample and the reference. Unfortunately, our THz TDS setup could not accurately replace the reference mirror in the same position as the sample mirror, resulting in large phase errors. An alternate method to determine the index of refraction was used to calculate the optical path length difference between the front and back reflections in the time domain. A diagram showing the geometry of the two THz signals is shown in Fig. 2. The average group refractive index is now defined by:

$$n_g = (T_b - T_f)c/2d = n_0 + \omega\left.\frac{dn}{d\omega}\right|_{\varpi} \tag{2}$$

where T_b is the time of the pulse off the back surface and T_f the time of the pulse off the front surface, c the speed of light, d the sample thickness, n_0 the average index of refraction, and ω the frequency. Since it has been demonstrated [10] that the index of refraction of polyimide is constant throughout the terahertz range of interest (0.2–2.5 THz), it is assumed that the group index is nominally equal to the phase index (i.e. $n_g = n_0$).

An alternate method to determine the absorption coefficient was also demonstrated. In reflection configuration, the pulses from the front and back surfaces could be isolated in the time domain and then a Fourier transform of each could be taken. The absorption coefficient $\alpha(\omega)$ could then be calculated using the following formula

$$\alpha(\omega) = -\frac{\cos(\theta_2)}{d}\ln\left(\frac{|r_{12}(\theta_1)E_{sam}(\omega)|}{|t_{12}(\theta_1)t_{21}(\theta_2)r_{23}(\theta_2)E_{ref}(\omega)|}\right) \tag{3}$$

in which $|E_{sam}(\omega)|$ is the magnitude of the THz field collected through the sample, $|E_{ref}(\omega)|$ the magnitude of the THz field collected through air, and each of the Fresnel coefficients shown in Fig. 2 is a function of the incident angle θ_1.

One of the problems with designing and maintaining aircraft is that the heat from jet engines can cause damage to the external structure of the aircraft. THz TDS in reflection configuration could be used to measure the material properties of the aircraft composites to determine if the composition of the material has fundamentally changed. Composite samples were prepared that were heated at various temperatures close to the maximum for the polyimide resin (~480 °C) for short durations. These samples are labeled 2 and 3 in Fig. 3. The first sample was burned at 440 °C for 4 min, creating a blister on the sample about 2 × 1.5 cm. The second sample was burned in two places: 430 °C for 6 min and 425 °C for 20 min.

Another goal of this research was to determine if various forms of damage could be imaged with a THz TDS system in reflection setup. In addition to the two burn samples, three other samples were prepared to assess the utility of a THz TDS system for NDE of damaged composites. The first composite sample, labeled 1 in Fig. 3, was used as a thickness standard to test THz TDS imaging techniques on various sample thicknesses. Another sample, labeled 5, consisting of two laminated pieces, was prepared to try to detect flaws. The bottom piece was prepared by etching four layers and then creating a 6 mm and a 3 mm flat bottom hole (~70 μm depth) in each of the four layers. A top layer was created by etching 4 layers with the same thicknesses and then attaching it to the bottom layer in the opposite direction with epoxy, being careful not to allow any epoxy into the voids. Finally, a third sample, labeled 4 in Fig. 3, was prepared by bending a piece of

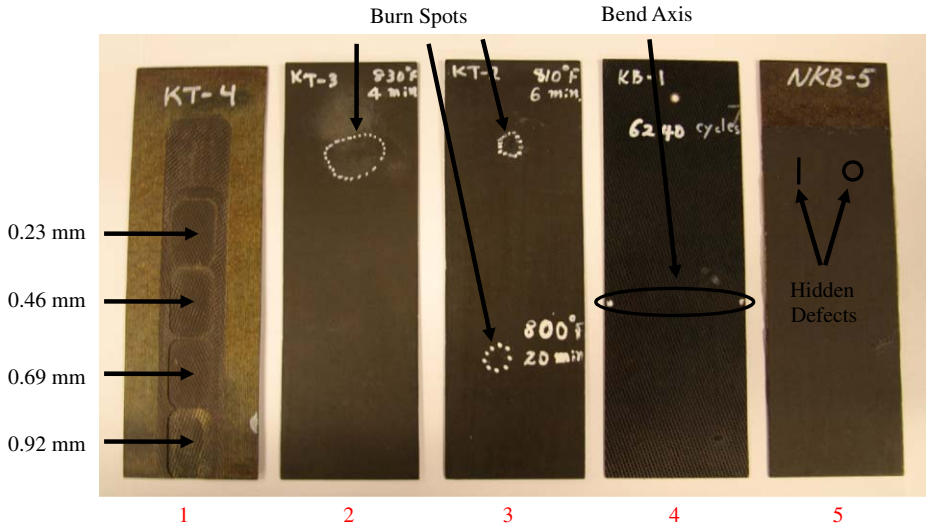

Fig. 3. Photograph showing the 5 composite samples: (1) thickness calibration sample, (2) & (3) burn samples, (4) mechanical stress sample, and (5) hidden defect sample showing the hidden location of two of the eight defects.

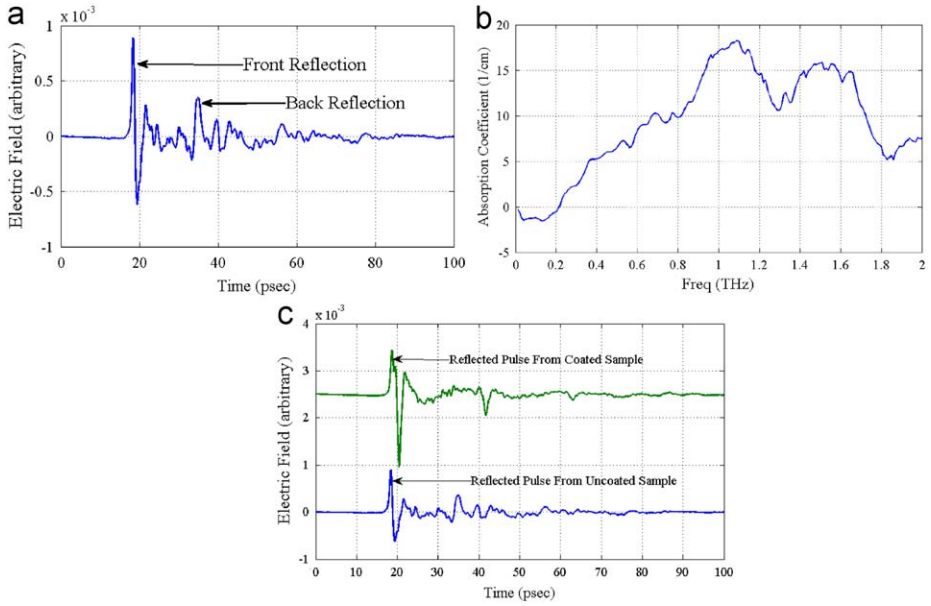

Fig. 4. THz TDS (a) pulses reflected from the front and back surface, (b) absorption coefficient for uncoated composite, and (c) a comparison of the pulse return from coated and uncoated composite.

glass fiber composite about a fixed axis a total of 6240 cycles to investigate bending damage with THz TDS imaging.

3. Results and discussion

3.1. Glass fiber composite material parameter measurements with reflection configuration

In preparation for measuring material parameters, we first measured a THz pulse reflected from the uncoated composite coupon in Fig. 4a. In Fig. 4a one can clearly see the initial reflection from the surface and the subsequent reflection off the back surface. The index of refraction was determined to be 2.03 ± 0.02 using Eq. (2). The absorption coefficient was then measured to be $7 \pm 2\,\mathrm{cm}^{-1}$ at 0.5 THz and $18 \pm 2\,\mathrm{cm}^{-1}$ at 1.0 THz with the results shown in Fig. 4b. This is comparable to other measurements made on composite samples in transmission configuration, where the index of refraction was 2.05–2.1 and the absorption coefficient was $12\,\mathrm{cm}^{-1}$ (at 0.5 THz) and $26–32\,\mathrm{cm}^{-1}$ (at 0.8 THz) [7]. Since the material parameters could be estimated in reflection mode, the next step was to determine if the technique could be used to diagnose chemical changes in the composite due to exposure to high temperature.

Unfortunately, the composite samples with burn damage had an exterior coating on them which caused an increase in the front reflection and a large decrease in the amplitude of the back reflection as shown in Fig. 4c. The exterior coating also caused a double reflection on the front surface from the coating and then the composite surface. A narrow dip can be seen in the positive portion of the first pulse, indicating the composite surface. Then the two reflections from the front add constructively in the

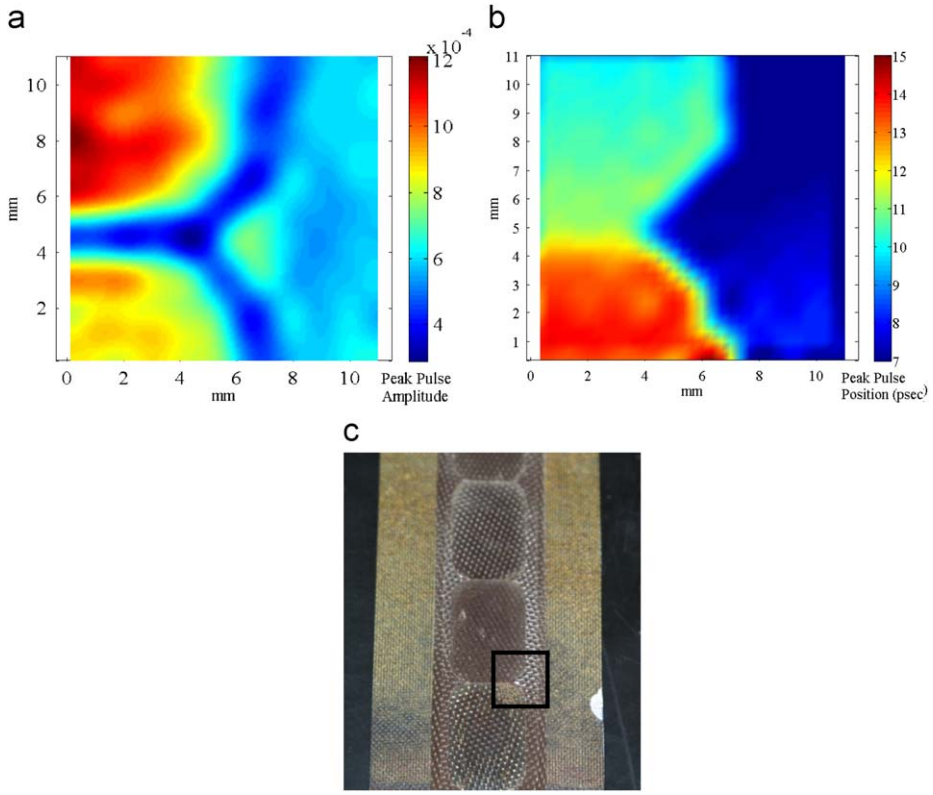

Fig. 5. THz TDS images showing a section of the composite milled to two different thicknesses using peak pulse amplitude (a) and peak pulse position (b) techniques. (c) Photograph of the calibration sample showing the scanned area.

negative polarity to create the larger negative maximum. The reflected pulse from the back of the composite was significantly reduced and, therefore, this technique was ineffective for measuring the material properties of the coated composite.

3.2. 2-D reflective imaging of glass fiber composite coupon defects

This subsection describes the THz imaging results from scanning the various defects outlined in Section 2. Imaging was accomplished using the THz TDS setup in Fig. 1 with a raster scanner to move the sample through the THz beam. The THz spot size was measured to be 3.5 mm and individual pixels were 1×1 mm in all of the scans. The first sample was prepared to calibrate the system based on material thickness. A THz image was taken of a 1×1 cm section of overlapping milled areas with different thicknesses. The image is shown in Fig. 5 where (a) represents the peak pulse amplitude and (b) shows the pulse position at each pixel [15]. The decrease in amplitude of the pulse at the edges is a result of THz scattering [15]. Similar images can be created using the area under the curve from the amplitude spectrum in the frequency domain. The different edge thicknesses of the milled areas cause a frequency dependence in amplitude intensity because the THz scattering from an edge is frequency dependent. The periodic modulation in Fig. 5b is a result of the interpolation technique to smooth out the pixels and does not match the pattern of the glass weave within the composite.

After imaging the calibration sample, the next task was to image the burn samples. The images of the burn samples formed by the peak amplitude of the THz pulses are shown in Fig. 6 with the visibly burned areas identified by the circles. Fig. 6a shows the sample that was burned at 440 °C for 4 min over $\sim 1.5 \times 2$ cm area. The sample has a bubble or blister on its exterior visible to the naked eye which roughly corresponds with the blue area within the black oval.

Comparisons of the THz time domain signal of pixels from the burn area were compared with those from outside the burn area. There are reflections within several of the pixels, showing evidence of air gaps. An example of the time domain signal from the pixel highlighted in Fig. 6a is shown in Fig. 7a. For comparison, a side profile of this burn is shown using an X-ray computed tomography image in Fig. 7b. The time delay between the two peaks equates to a distance of 480 μm. This is roughly equivalent to the 500 μm difference measured between the burn blister and the undamaged sample using a micrometer. The other two burn areas are shown in Fig. 6b and c, neither of which showed much visual evidence of blistering. The dark red area within the circle in 6b is roughly equivalent to the position of the residue in the burn area. The red circular dots in 6c correspond to the white marker dots (see Fig. 6f) made on the samples to show the extent of the burn area. The THz image of the damage area in 6c was inconclusive in showing evidence of burning.

Next, the sample with the mechanical damage caused by bending the composite 6240 cycles was imaged in reflection setup. The image of the sample in Fig. 8 was constructed using the area under the curve from the amplitude spectrum between 1.2 and 1.4 THz. There is perhaps a slightly greater density of lower amplitude radiation around the bend axis, but it is difficult to categorize as conclusive.

Voids were also investigated, which simulate either manufacturing defects or damage. The results of a THz image are shown in Fig. 9 for a circular void (3×3 mm). For the circular void, an

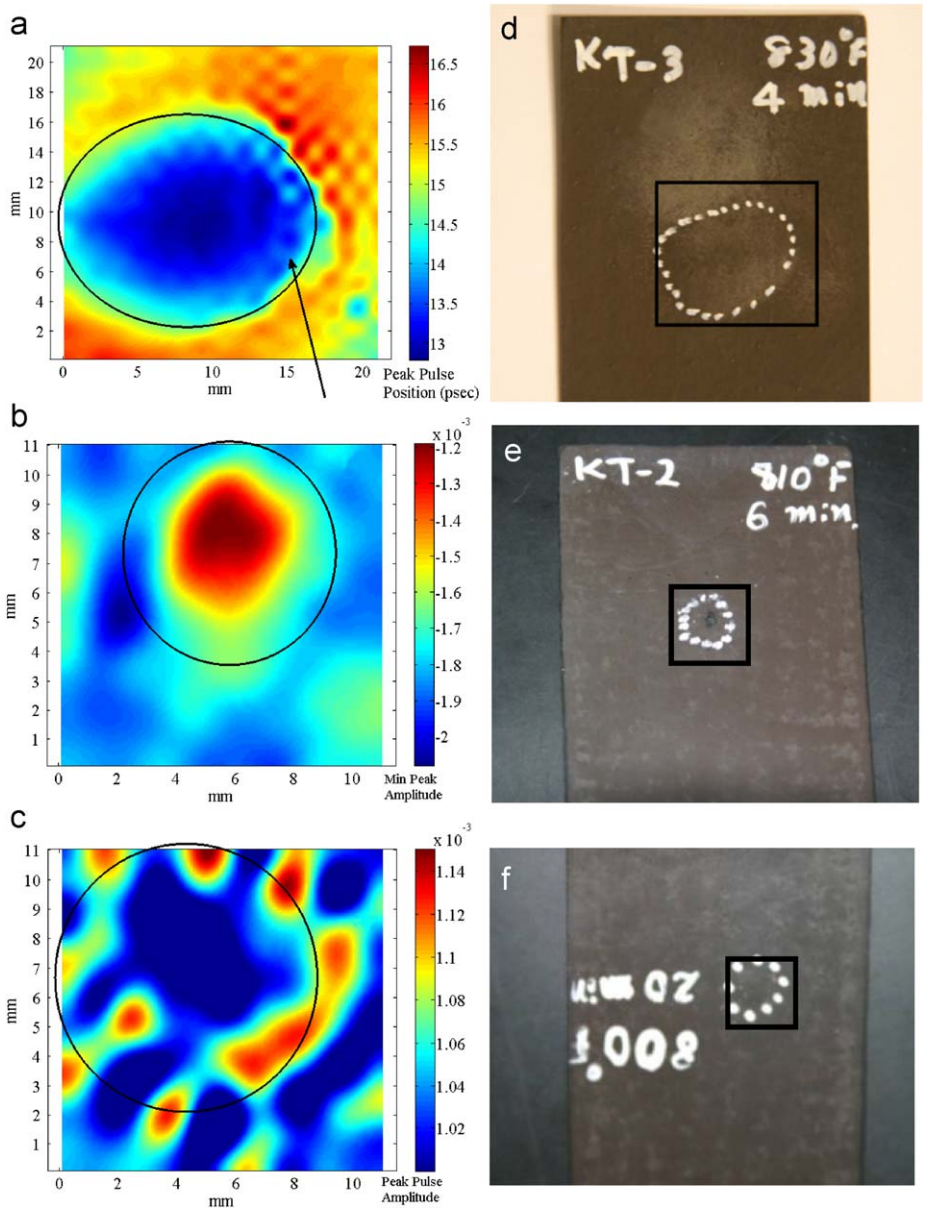

Fig. 6. THz TDS images and photos for three burn areas on composite samples: (a), (d) 440 °C for 4 min; (b), (e) 430 °C for 6 min; and (c), (f) 425 °C for 20 min.

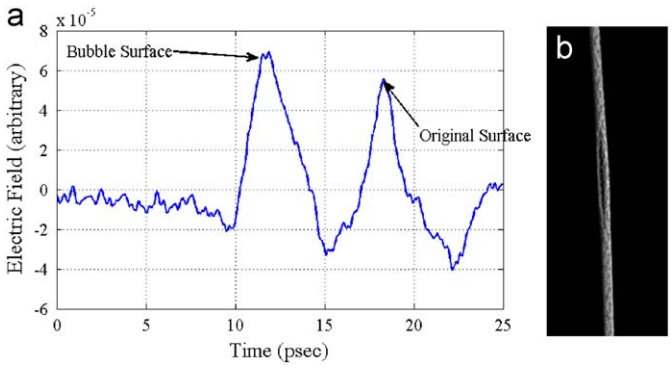

Fig. 7. (a) THz TDS time domain signal showing the THz signal collected from the pixel located in Fig. 6(a). (b) An X-ray computed tomography scan of the side profile of the large burn dot.

imaging technique was used which measured the relative amplitude of the first Fabry–Perot reflection after the main pulse in the time domain. An X-ray computed tomography image of the composite sample is shown in 8b, which shows the positions of the hidden circular and slit voids. The same technique could not conclusively locate the slit void.

3.3. 2-D reflective imaging of glass fiber composite panel defects

In the previous subsection, all of the THz images were taken on thin coupons of composite with various forms of damage. On an aircraft, the composite strips are attached to both sides of a much thicker honeycomb structure which is then attached as an external part of the aircraft. A THz TDS transmission scan was attempted on an entire panel (~3 cm thick), however, very little of

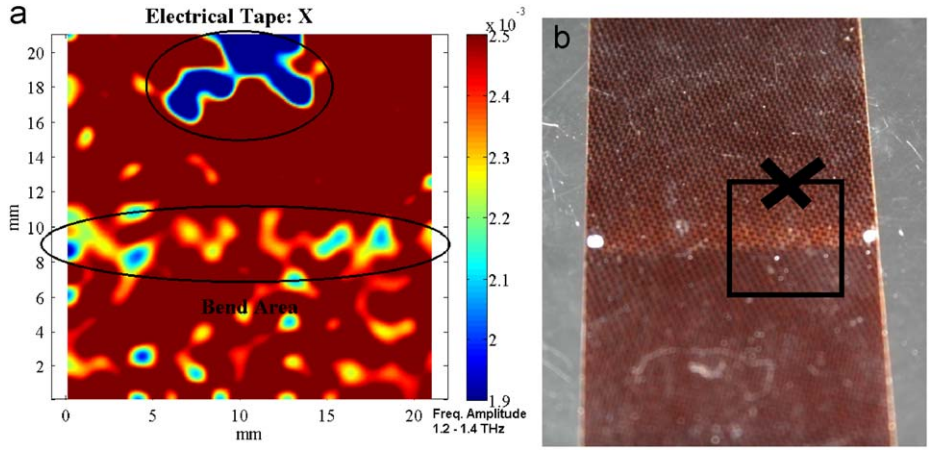

Fig. 8. . (a) THz TDS reflection image using the amplitude of frequencies (1.2–1.4 THz) showing bend damage across the central bend axis and (b) photo of scanned area.

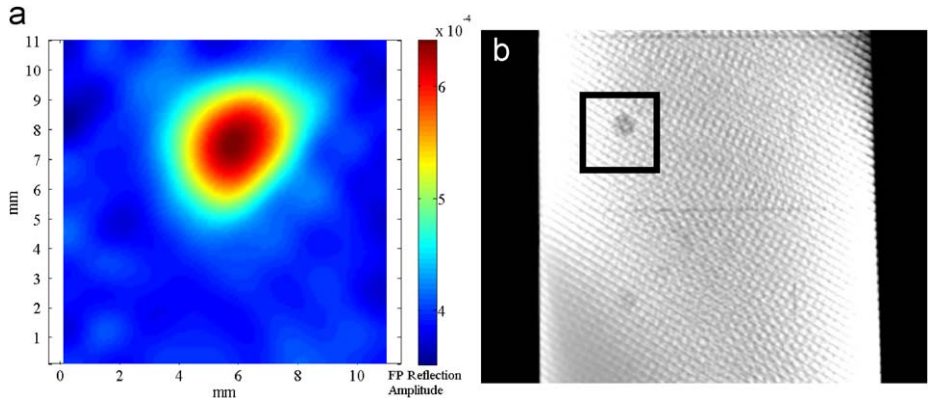

Fig. 9. THz TDS images showing 3 mm diameter milled circle hidden between two composite strips using first Fabry–Perot reflection (a). X-ray computed tomography image showing the position of the hidden circular and slit voids (b).

the energy penetrated through. Obviously, TDS reflection mode would be required to detect damage to such a panel. Two panels were prepared for imaging and analysis with THz radiation: one with burn damage and holes punched in its surface and another panel with a portion of its paint removed with a butanane solvent.

The first panel had holes (4.5 mm diameter) punched through the composite representing puncture damage and burn damage between the holes. The scanned area of the panel included one hole and two burn areas (see Fig. 10a–c). A very noticeable burn area is located on the right half. The other burn area is much less noticeable to the naked eye; in fact, it was not noticed until it was revealed in the THz TDS image. THz images of the panel can be seen in Fig. 10, where the (a) minimum peak amplitude, (b) maximum peak position, and (c) amplitude spectrum (1.4–1.6 THz) were used to construct the images. The second panel had a solvent, butanane, applied to the exterior surface of the panel to dissolve away the paint. The area that was dissolved was about 7 mm wide and can be seen in Fig. 10d. Both of these two samples represent types of external damage that could occur to the panels.

Another important question was how the honeycomb structure under the composite reflects the THz signal and whether defects within the honeycomb structure could be detected. Long, time duration scans were taken of an entire panel to see whether there were any reflections within the honeycomb. A typical plot of the first half of a long scan is shown in Fig. 11a where the time domain reflections of a coated and uncoated composite surface are shown. Apart from the ZnTe etalon effect, there is nothing remarkable about the pulse characteristics even when it was extended to 200 ps. Apparently, the honeycomb either traps the energy or it is attenuated sufficiently such that the reflected signal is not observable. There is also no back reflection from the back surface of the composite, indicating a smooth transition from the composite to the honeycomb. A graph of the corresponding frequency spectra in Fig. 11b shows the relatively stronger amplitude of the THz signal reflected from the uncoated surface.

3.4. Depth of discontinuities analysis using reflection configuration

Depth analysis was performed on data collected on the delaminated portion of the sample labeled 5 in Fig. 3. During the data collections it was quickly apparent that the adhesive–composite interface provided a large enough index discontinuity to create a back reflection. The air–composite interface provided a large reflected signal because the greater Δn resulted in a higher reflection coefficient. Fig. 12 shows two examples of the time domain pulse returns showing the reflections from the two discontinuities. The ZnTe (n=3.2, thickness=1 mm) reflection was measured at the same position ($\sim$21 ps after the main pulse) on all of the temporal plots and was clearly distinguishable from the back reflection of the composite sample. The polarity of the ZnTe reflection was not reversed from the main pulse while the polarity of the back reflection was reversed because of the difference in the change of index of refraction at the interface.

A Fourier method was used to show the depth of delaminations in the laminated sample. This technique $D(t)$ is

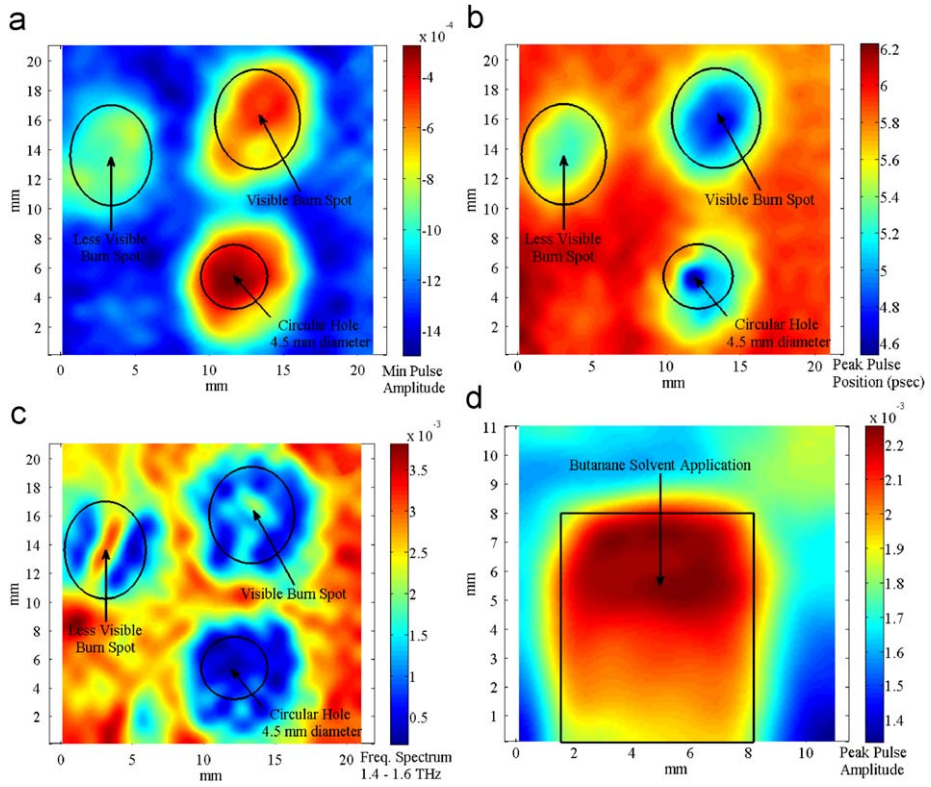

Fig. 10. THz TDS reflection setup image of entire panel with puncture hole (4.5 mm diameter) and two burn blisters. Images were constructed using the (a) minimum peak pulse amplitude, (b) maximum peak pulse position and (c) the frequency spectrum amplitude added under the curve (1.4–1.6 THz). (d) THz TDS image of a panel with the exterior coating removed with butanane solvent.

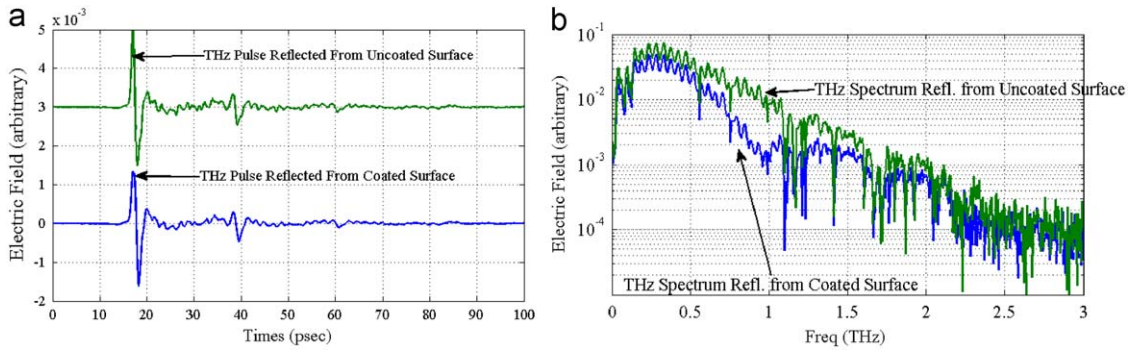

Fig. 11. THz TDS (a) time domain plots and (b) frequency spectra for a coated and uncoated surface of an aircraft panel.

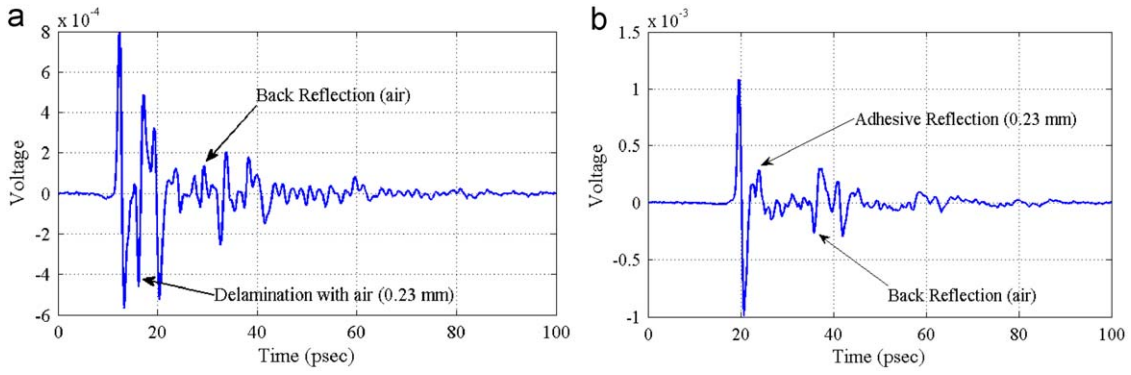

Fig. 12. THz TDS time domain plots showing reflections from discontinuities: (a) air and (b) adhesive.

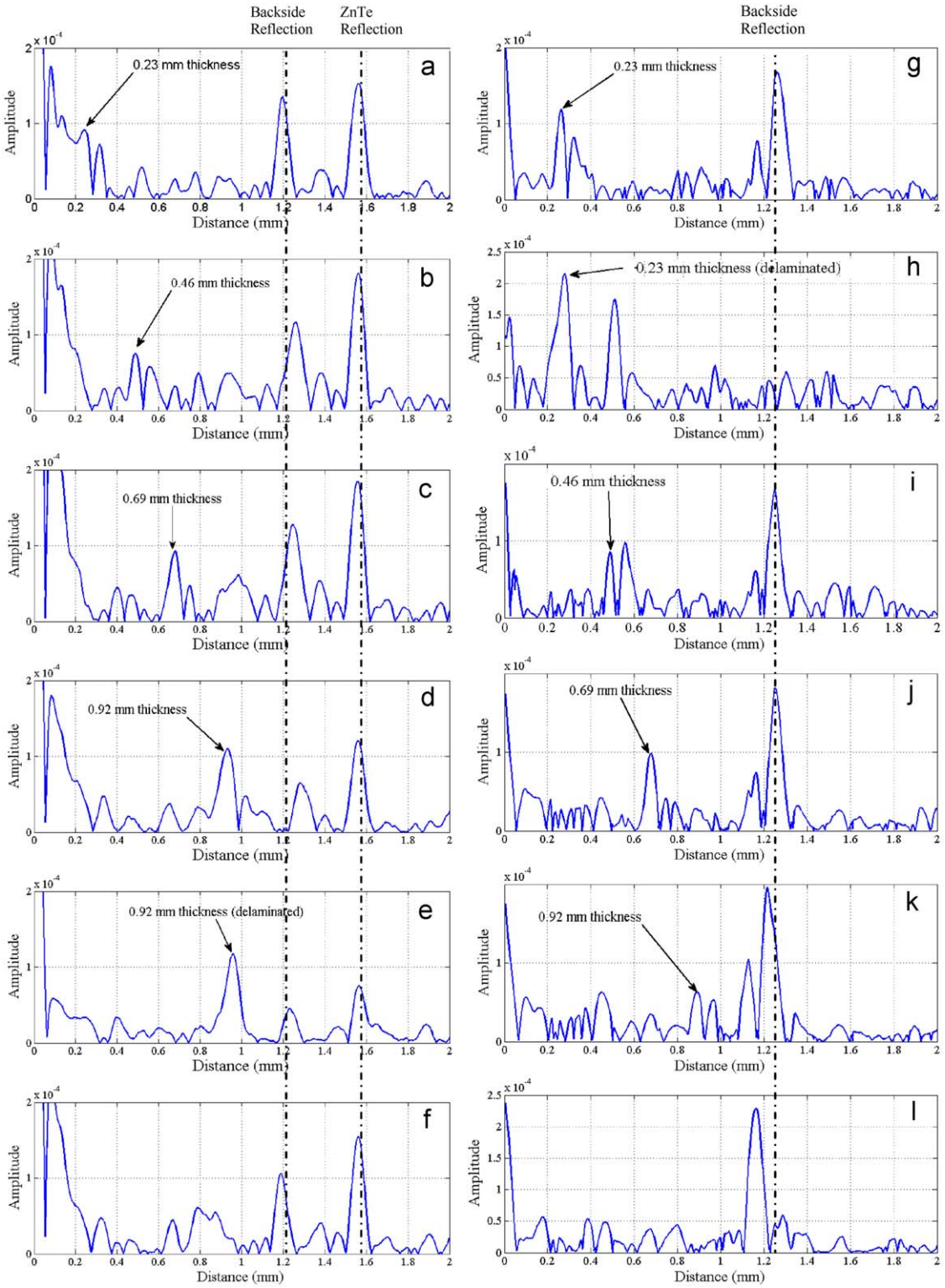

Fig. 13. Results using the Fourier technique in Eq (4) showing the discontinuities present in a composite sample laminated at various thicknesses: (a) 0.23 mm, (b) 0.46 mm, (c) 0.69 mm, (d) 0.92 mm, (e) 0.92 mm delaminated and (f) no lamination. Results using the Fourier technique with the TDS system characteristics subtracted are shown next. The various thicknesses were measured in the opposite direction: (g) 0.23 mm, (h) 0.23 mm delaminated, (i) 0.46 mm, (j) 0.69 mm, (k) 0.92 mm and (l) no lamination.

demonstrated in the following equation:

$$D(t) = |ifft|fft(E(t))|| \tag{4}$$

in which *fft* is the fast Fourier transform and *ifft* the inverse fast Fourier transform. A comparison of the returns from discontinuities at various depths is shown in Fig. 13a–f. The dashed lines were added to show the similarity of the backside reflections in each scan along with the pulse reflection from the ZnTe etalon effect. A separate calculation was made to remove the TDS system effects. This was accomplished by making a

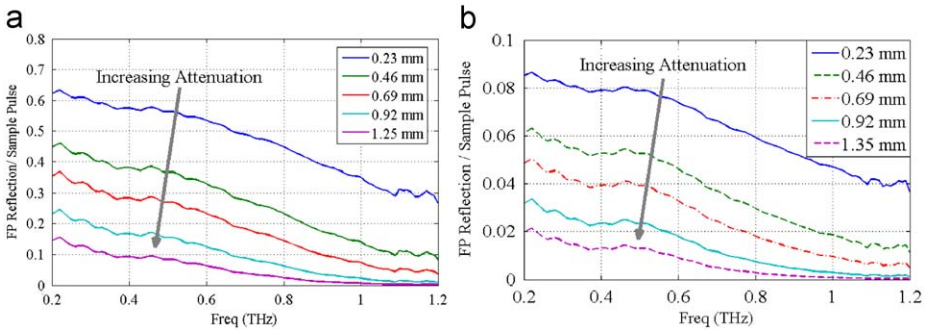

Fig. 14. Chart showing the calculated relative strength of the first Fabry–Perot reflection after traveling through various thicknesses of composite material for THz TDS (a) reflection configuration and (b) transmission configuration.

separate measurement of the THz pulse reflection from aluminum and then subtracting out the aluminum transfer function from the sample. This procedure removed most of the main pulse and the ZnTe reflection. A series of depth measurements can be seen in Fig. 13g–l for the various thicknesses. Each series of plots was measured from a different side of the sample, showing minimal difference from each side.

The attenuation of the THz signal can be estimated based on the measured absorption coefficient of the composite and the Fresnel coefficients from the two air–sample interfaces. To show the relative strength of the first Fabry–Perot etalon reflection to the surface reflection, the following equation was used

$$\frac{E_{FP\_Ref}}{E_{sam}} = \frac{t_{12}(\theta_1)t_{21}(\theta_1)r_{23}(\theta_1)}{r_{12}(\theta_1)} \exp\left(-\frac{\alpha(\omega)}{2}(2d)\right) \tag{5}$$

where the Fresnel coefficients geometry was shown previously in Fig. 2 and are defined by

$$r_{12} = \frac{n_1\cos(\theta_1) - n_2\cos(\theta_2)}{n_1\cos(\theta_1) + n_2\cos(\theta_2)}, \quad t_{12} = 1 + r_{12} \tag{6}$$

$$r_{23} = \frac{n_2\cos(\theta_2) - n_3\cos(\theta_3)}{n_2\cos(\theta_2) + n_3\cos(\theta_3)}, \quad t_{21} = 1 + r_{21} \tag{7}$$

The graph in Fig. 14a shows the relative strength of the first Fabry–Perot reflection at various depths from an air–composite discontinuity to the strength of the front pulse. These relative amplitudes of the Fabry–Perot reflections compared favorably with the amplitudes of the measured data from the laminate sample. A similar chart is shown for an air–composite interface in Fig. 14b in transmission configuration [10].

4. Conclusions

An aircraft composite with various forms of damage was examined using a reflective THz time domain spectroscopy (TDS) system. Indices of refraction and absorption coefficients in the terahertz frequency range for composite were measured using a reflection configuration, however, the addition of a coating reduced the back reflection and prevented the technique from being used for nondestructive analysis. THz TDS reflection imaging on the composite strips in Fig. 3 was performed first. Burn spots and a hidden circular void could be identified in a THz image, but there was little evidence that areas of damage from mechanical bending stress and simulated hidden cracks could be detected with terahertz TDS reflective imaging. Next, THz TDS reflective configuration was used to image an entire panel, consisting of two composite strips surrounding a honeycomb center. Surface damage, such as puncture holes, burn spots, and paint removal could be detected, but no reflections occurred below the thin composite layer down into the honeycomb. The approximate depth of delamination could be determined in the time domain by measuring the timing of a Fabry–Perot reflection through a thin slice of the composite.

Terahertz radiation can exhibit some unique characteristics for nondestructive evaluation from other forms of electromagnetic radiation. Microwaves have the ability to penetrate composites, but their spatial resolution is more limited due to their longer wavelengths. Infrared techniques can have better spatial resolution than terahertz, but less penetration depth. THz can penetrate composite without contacting it, with submillimeter transverse resolution, and can detect surface defects, hidden voids, delaminations, and bending damage in composites. The depth resolution for defects is much better than the spatial resolution, and thin composite samples can be analyzed with THz TDS.

There are advantages and disadvantages to using either the TDS transmission or reflection configuration. It was easier to get a smaller THz spot size onto the sample using a transmission configuration. This was primarily due to the large ratio of focal length to diameter in the parabolic mirrors and the cumbersome stages used to steer them. Custom optical parts could alleviate this problem for reflection configurations. It was also easier to measure the material properties of the composite using a transmission configuration. With an exterior coating, the reflective technique for measuring the material properties was ineffective. Reflection mode is certainly a more likely candidate for a maintenance technique, as was mentioned earlier, but transmission setup could aid in the design and quality control of glass fiber composites. Reflection mode would also be a more effective technique in determining the depth of delaminations. This is due to reflection mode signals traveling a shorter distance through the attenuating composite and due to the relative similarity in the amplitude of Fresnel reflections between a void and the initial pulse. This can be easily seen from the calculations plotted in Fig. 14. The relative amplitude of the first Fabry–Perot reflection is calculated to be an order of magnitude larger in reflection configuration than in transmission.

Acknowledgements

The glass fiber composite samples used in this research were provided by the Air Force Research Laboratory Materials and Manufacturing Directorate, Wright Patterson AFB, OH. This research was partially funded by the Air Force Office of Scientific Research.

References

[1] Chan WL, Deibel J, Mittleman DM. Imaging with terahertz radiation. Rep Prog Phys 2007;70:1325–79.

[2] Cooney A, Blackshire JL. Advanced imaging of hidden damage under aircraft coatings. Advanced sensor technologies for nondestructive evaluation and structural health monitoring II. Proc SPIE 2006;6179:617902.
[3] Redo-Sanchez A, Karpowicz N, Xu J, Zhang XC. Damage and defect inspection with terahertz waves. In: The 4th International Workshop on Ultrasonic and Advanced Methods for Nondestructive Testing and Material Characterization 2006, p. 67–77.
[4] Zimdars D, White J, Stuk G, Chernovsky A, Fichter G, Williamson S. Large area terahertz imaging and non-destructive evaluation applications. In: The Fourth International Workshop on Ultrasonic and Advanced Methods for Nondestructive Testing and Material Characterization, UMass Dartmouth, N. Dartmouth, MA, 2006.
[5] Wang S, Zhang XC. Pulsed terahertz tomography. J Appl Phys D 2004;37: R1–36.
[6] Wietzke D, Jordens C, Krumbholz N, Baudrit B, Bastian M, Koch M. Terahertz imaging: a new non-destructive technique for the quality control of plastic weld joints. J Euro Opt Soc 2007;2:07013.
[7] Rutz F, Koch R, Khare S, Moneke M, Richter H, Ewert U. Terahertz quality control of polymeric products. Int J Infrared and Millim Waves 2006;27: 547–56.
[8] Rutz F, Hasek T, Koch M, Richter H, Ewert U. Terahertz birefringence of liquid crystal polymers. Appl Phys Lett 2006;89:221911.
[9] Reiten MT, Hess L, Cheville RA. Nondestructive evaluation of ceramic materials using terahertz impulse ranging. Proc SPIE 2006;617905:1–8.
[10] Stoik CD, Bohn MJ, Blackshire JL. Nondestructive evaluation of aircraft composites using transmissive terahertz time domain spectroscopy. Opt Express 2008;16:17039–51.
[11] Wietzke S, Jansen C, Rutz F, Mittleman DM, Koch M. Determination of additive content in polymeric compounds with terahertz time-domain spectroscopy. Polym Test 2007;26:614–8.
[12] Jackson JB, Mourou M, Whitaker JF, Duling IN, Williamson SL, Menu M, et al. Terahertz imaging for non-destructive evaluation of mural paintings. Opt Commun 2008;281:527–32.
[13] Fletcher JR, Swift GP, Dai D, Chamberlain JM, Upadhya PC. Pulsed Terahertz Signal Reconstruction. J Appl Phys 2007;102:113105.
[14] Jepsen PU, Jensen JK, Moller U. Characterization of aqueous alcohol solutions in bottles with thz reflection spectroscopy. Opt Express 2008;16: 9318–31.
[15] Mittleman DM. Sensing with Terahertz Radiation. In: Mittleman DM, editor. New York, NY: Springer; 2003.